8-21-2000

Low-Mass Spectroscopic Binaries in the Hyades: A Candidate Brown Dwarf Companion

I. Neill Reid
University of Pennsylvania

S. Mahoney
Dartmouth College

Mon. Not. R. Astron. Soc. **316**, 827–844 (2000)

Low-mass spectroscopic binaries in the Hyades: a candidate brown dwarf companion

I. Neill Reid[1]★ and S. Mahoney[2]

[1]*Department of Physics and Astronomy, University of Pennsylvania, 209 S. 33rd Street, Philadelphia, PA 19104-6396, USA*
[2]*Hinman Box 1709, Dartmouth College, Hanover, NH 03755, USA*

Accepted 2000 March 22. Received 2000 March 13; in original form 2000 January 31

ABSTRACT

We have used the HIRES echelle spectrograph on the Keck I telescope to obtain high-resolution spectroscopy of 51 late-type M dwarfs in the Hyades cluster. Cross-correlating the calibrated data against spectra of white dwarfs allows us to determine heliocentric velocities with an accuracy of $\pm 0.3\,\mathrm{km\,s^{-1}}$. 27 stars were observed at two epochs in 1997; two stars, RHy 42 and RHy 403, are confirmed spectroscopic binaries. RHy 42 is a double-lined, equal-mass system; RHy 403 is a single-lined, short-period binary, $P \sim 1.275$ d. RHy 403A has an absolute magnitude of $M_I = 10.85$, consistent with a mass of $0.15\,\mathrm{M_\odot}$. The systemic mass function has a value $[M_2 \sin(i)]^3/(M_1 + M_2)^2 = 0.0085$, which, combined with the non-detection of a secondary peak in the cross-correlation function, implies $0.095 > M_2 > 0.07\,\mathrm{M_\odot}$, and the strong possibility that the companion is the first Hyades brown dwarf to be identified. Unfortunately, the maximum expected angular separation in the system is only $\sim$0.25 mas. Five other low-mass Hyads are identified as possible spectroscopic binaries, based either on repeat observations or on a comparison between the observed radial velocity and the value expected for Hyades cluster members. Combined with *HST* imaging data, we infer a binary fraction between 23 and 30 per cent. All of the stars are chromospherically active. RHy 281 was caught in mid-flare and, based on that detection, we estimate a flaring frequency of $\sim$2.5 per cent for low-mass Hyades stars. Nine stars have rotational velocities, $v \sin(i)$, exceeding $20\,\mathrm{km\,s^{-1}}$, and most of the sample have detectable rotation. We examine the Hα emission characteristics of low-mass cluster members, and show that there is no evidence for a correlation with rotation.

Key words: stars: chromospheres – stars: late-type – stars: low-mass, brown dwarfs – open clusters and associations: individual: Hyades.

1 INTRODUCTION

The frequency of binary and multiple systems amongst stars of different masses is a fundamental parameter in both star formation theory, and understanding mechanisms for the formation of planetary systems. Low-mass stars have received less attention than solar-type G dwarfs, but the available observations suggest that the multiplicity fraction decreases from $\sim$70 per cent or more at $M \sim 1\,\mathrm{M_\odot}$ (Duquennoy & Mayor 1991) to $\sim$35 per cent for M dwarfs (Fischer & Marcy 1991; Reid & Gizis 1997a). Most previous surveys have concentrated on field stars, which span a range of age and abundance. Open clusters offer an alternative laboratory, where age and abundance are both homogeneous and, within the limits of theoretical models, known factors. Cluster analyses, however, must allow for the possibility that dynamical evolution may have modified key characteristics since formation. Binaries, for example, are likely to be retained preferentially, inflating the apparent binary frequency at a given spectral type.

The Hyades is the nearest substantial open cluster, and its members have received considerable observational and theoretical attention. Higher mass cluster members (spectral types earlier than mid-K) have been the subject of both radial velocity observations (Griffin et al. 1988) and high-resolution infrared speckle interferometry (Patience et al. 1998), as well as extensive proper motion surveys capable of detecting wide companions (Hanson 1975; Reid 1992, and references within). The deduced binary frequency is broadly consistent with Duquennoy & Mayor's (1991) analysis of similar-mass stars in the solar neighbourhood. At lower masses, over 50 of the cluster M dwarfs were targetted for observation by the *Hubble Space Telescope* (*HST*) (Gizis & Reid 1995; Reid & Gizis 1997b), with the Planetary Camera images providing a spatial resolution comparable to the ground-based speckle data, $\Delta \sim 0.1$ arcsec. Again, the frequency of companions is consistent with that amongst nearby field dwarfs,

★ E-mail: inr@morales.physics.upenn.edu

Table 1. Hyades cluster members.

RHy	Other	V	$(V-I)$	M_V	r (pc)	Comments
9	LP 357-86	16.73	3.18	13.45	45.3	unresolved *HST*
23	LP 414-30	16.18	3.01	12.74	48.8	unresolved
42	LP 414-794	15.30	2.93	12.04	44.9	unresolved
46	LP 414-51	16.68	3.12	13.09	52.4	unresolved
49AB	LP 414-50	15.89	3.04	12.51	47.5	*HST* binary, $\Delta = 0''.36$, δI 1.6
60	LP 414-110	16.12	3.14	12.50	52.9	unresolved
64		16.33	3.23	13.65	36.3	unresolved
83		17.46	3.52	14.69	35.8	unresolved
88A		13.06	1.90	9.13	61.2	binary, $\Delta = 5''$
88B		14.11	2.60	10.18	61.2	
98	LP 414-1570	16.63	3.22	13.64	36.8	unresolved
101	LP 474-1606	17.11	3.46	14.20	37.9	unresolved
115		16.50	3.03	12.74	56.4	unresolved
119AB	LP 414-138	17.29	3.54	14.16	42.3	*HST* binary, $\Delta = 0''.88$, δI 0.1
126	LP 414-1895	17.33	3.38	13.55	37.8	unresolved
129	LP 474-217	15.33	2.86	12.40	38.5	unresolved
132	vA 94	15.83	3.03	12.30	50.8	unresolved
143	vA 127	16.23	3.02	12.83	37.9	unresolved
158	LP475-14	16.31	3.20	13.07	44.5	unresolved
162		16.54	3.21	13.63	38.2	unresolved
163	vA 213	15.44	3.00	12.48	39.1	unresolved
165	LP 415-19	19.67	4.34	16.41	44.9	unresolved
182	LP 4156-35	15.89	3.06	12.53	47.0	unresolved
199	LP 415-50	16.70	3.22	13.42	45.3	unresolved
200	LP 475-59	16.07	2.89	12.56	50.3	unresolved
202AB	LP 415-51	16.70	3.11	13.34	37.0	*HST* binary, $\Delta = 0''.28$, δI 1.8
219	vA 352	16.37	2.87	13.03	46.6	unresolved
221AB	LP 415-71	15.88	3.10	12.54	46.7	*HST* binary, $\Delta = 0''.31$, δI 0
230	LP 415-881	18.25	3.42	14.72	38.7	unresolved
231	LP 415-875	15.89	3.11	12.49	38.6	unresolved
240 A		18.77	3.72	15.39	47.5	binary, $\Delta = 2''.5$, δI 0
240 B		18.96	3.82	15.59	47.5	
242	vA 432	15.91	2.92	12.55	47.0	unresolved
244AB	LP 415-108	15.64	2.97	12.07	51.8	*HST* binary, $\Delta = 0''.14$, δI 1.1
260	Ha 430	16.40	3.07	13.52	37.6	unresolved
281	LP 415-142	18.12	3.30	14.39	55.8	unresolved
297	LP 475-1012	17.04	3.18	13.42	52.9	unresolved
298	vA 616	15.90	2.93	12.66	44.5	unresolved
301	LP 475-125	16.53	3.15	13.43	41.6	unresolved
331	LP 415-206	16.43	2.99	13.30	42.3	unresolved
346AB	LP 475-176	16.03	3.18	12.84	43.4	*HST* binary, $\Delta = 0''.48$, δI 0.4
367		16.45	3.13	12.94	50.3	unresolved
369	LP 475-1419	16.14	2.92	12.59	51.3	unresolved
371AB	LP 415-266	15.36	3.10	12.02	46.6	*HST* binary, $\Delta = 0''.17$, δI 1.3
376	LP 415-1692	15.80	2.90	12.52	45.3	unresolved
377AB	LP 475-214	16.24	3.15	12.65	52.4	binary *HST*, $\Delta = 1''.66$, δI 1.0
386	LP 415-2128	18.83	3.69	15.66	43.0	unresolved
390	LP 415-1773	18.49	3.83	15.13	47.0	unresolved
391		16.42	3.35	13.08	46.6	unresolved
399	LP 415-1816	15.09	2.92	12.18	38.2	unresolved
402		17.77	3.25	13.94	58.4	unresolved
403	LP 415-327	18.04	3.47	14.42	52.9	unresolved
	G8-17	12.68		9.3		unresolved

although only six binaries are available for this statistical comparison.

Few accurate radial velocity measurements exist for late-type Hyades dwarfs. Griffin et al. (1988) include a few late-K and early-M dwarfs in their survey, and Cochran & Hatzes (1999) include early-type M dwarfs in their planet search. Stauffer et al. (1997) surveyed 49 early-type M dwarfs, including three non-members, identifying seven double-lined spectroscopic binaries and one triple system. The faintest star in their sample, vA 127 (RHy 143), has spectral type M4 and an absolute magnitude $M_V = 12.83$. Data for later type stars are scarce. Jones, Fischer & Stauffer (1996) include three of the lowest luminosity cluster members (Br 804 = RHy 386, Br 816 and Br 262 = LP415-20, from Bryja et al. 1993) in their high-resolution spectroscopy of low-mass Hyads and Pleiads. Most recently, Terndrup et al. (2000) have observed 18 Hyades dwarfs with $M_V > 11$, including 10 in common with the current sample.[1]

Given the paucity of observations, it is not surprising that few spectroscopic binaries have been identified amongst the cluster M dwarfs. Extending observations to cover this smaller range of physical separations provides a further comparison of the binary frequency relative to that amongst field dwarfs. In addition, high-resolution spectroscopic data provide a means of probing the

[1] Note that the stars designated Re by Terndrup et al. should be identified using the prefix RHy.

physical structure of these stars, notably the range of chromospheric activity and the distribution of rotational velocities. The current scarcity of observations reflects the faint apparent magnitudes of these stars, and the consequent difficulties of obtaining high signal-to-noise data at the appropriate spectral resolution. Those circumstances have changed with the availability of 8–10 metre telescopes equipped with high-efficiency echelle spectrographs.

This paper presents the first results from a survey of late-type Hyades M dwarfs, based on observations with the HIRES spectrograph on the Keck I telescope. Most of the targets also have high-spatial-resolution *HST* images. The following section outlines the observations; Section 3 describes the measurement of radial and rotational velocities; Section 4 presents the techniques used to identify possible binaries; Section 5 discusses the binaries identified from our observations; Section 6 compares rotation and activity in these low-mass stars; and Section 7 presents our conclusions.

2 OBSERVATIONS

We have obtained high-resolution spectroscopy of 53 late-type members of the Hyades cluster using the HIRES echelle spectrograph (Vogt et al. 1994) on the Keck I telescope. The observations were made in the course of three allocations: a one-night run, 1997 January 13 (UT); over the three-night period December 10 to 12 in the same year; and on 1999 December 29 and 30. Conditions were clear and photometric throughout, with subarcsecond seeing. All of the target stars except G8-17 are drawn from Reid's (1993) list of stars with both proper motions and photometry consistent with Hyades membership. G 8-17 is listed as a candidate Hyades member in the Lowell survey (Giclas, Burnham & Thomas 1972), and the star has *UBV* photometry by Sandage & Kowal (1986). Our spectrum confirms it as a Hyades member. The majority of these stars were included in Reid & Gizis's (1997b) *HST* Planetary Camera imaging programme, which embraced Hyades members with $M_V > 11.9$ (spectral types later than M3). Several are therefore known to be spatially resolved binary systems. Table 1 lists photometric data, from Reid (1993) and Leggett, Harris & Dahn (1994), for stars in the present sample. Individual distances are estimated from the proper motions using the convergent-point method and the results from Perryman et al.'s (1998) *Hipparcos* analysis (see Section 4). These values are typically 5 per cent smaller than distances cited in Reid (1993).

In addition to the Hyades members, we obtained observations of field M dwarfs of comparable spectral types, as well as several candidate Hyads which prove to be non-members. Photometry and spectral types for those stars are listed in Table 2, together with heliocentric velocity measurements, both from the published literature (Marcy & Benitz 1989; Delfosse et al. 1998) and from our own observations. One of the Hyades non-members, RHy 80, is a double-lined spectroscopic binary, Table 2 lists velocity measurements at two epochs.

Our observations were made using a 0.86-arcsec slit, which gives a resolution of 45 000, or 6.67 km s^{-1}. With an echelle angle of $-0\overset{\circ}{.}18$ and a cross-disperser angle of $1\overset{\circ}{.}37$, the spectra provide partial coverage of the wavelength region from 6350 to 8730 Å in 16 orders, including Hα and the atmospheric A- and B-bands. We adopted a standard exposure time of 600 s for stars with $13 < V < 17$, increasing the integration time to between 900 and 1800 s for fainter stars.

The images were flat-field-calibrated and bias-subtracted in the usual manner, and the spectral orders were extracted using software written by T. Barlow. The wavelength calibration was

Table 2. Field M dwarfs.

Name	M_V	$(V-I)$	Spectral type	$V_{\rm hel}$ km s^{-1}	References	$V_{\rm hel}$ km s^{-1}	MJD 50400+
Gl 54.1	14.17	3.15	M4.5		L92, RHG	28.0 ± 0.10	60.20727
Gl 83.1	14.02	3.12	M4.5	−29	L92, RHG, D98	-28.6^{ref}	60.20251
						-28.6^{ref}	11541.17607
						-28.6^{ref}	11542.18446
Gl 234 A	13.01	3.02	M4.5	12	L92, RHG	14.85^{ref}	793.59378
						16.2 ± 0.12	11542.46873
LP 771-95	11.9		M3.5		RHG	−1.2 ± 0.13	60.21650
LP 771-96A	12.5		M4		RHG	−5.5 ± 0.18	60.21946
Gl 402	12.46	2.79	M4	−1.1	L92, RHG, MB89	−1.1 ± 0.20	792.66871
Gl 445	12.17	2.64	M4		L92, RHG	−111.5 ± 0.25	794.67419
Gl 447	13.50	2.98	M4	−31.34	L92, RHG, MB89	−31.2 ± 0.24	794.66546
						−31.3 ± 0.24	11541.56632
Gl 831AB	12.50	2.99	M4.5	−57.1	L92, RHG, MB89	−58.75 ± 0.30	793.19816
Gl 876	11.82	2.74	M4	−1.77	L92, RHG, MB89	−1.95 ± 0.25	793.21099
RHy 80A		3.17	M4.5		R93	0.88 ± 0.25	60.37904
RHy 80B		3.2	M4.5		R93	29.12 ± 0.42	
RHy 80A		3.17	M4.5		R93	2.35 ± 0.25	792.34271
RHy 80B		3.2	M4.5		R93	26.4 ± 0.35	
RHy 110		3.03	M4		R93	60.67 ± 0.25	60.42207
RHy 225		2.76	M3		R93	40.25 ± 0.31	792.54615
RHy 254		3.22	M4		R93	−4.12 ± 0.20	60.25284

Column 6 identifies the source of the photometry, spectroscopy and radial velocity measurements listed in columns 2 to 5.
L92: photometry from Leggett (1992).
R93: photometry/spectral type from Reid (1993).
RHG: spectral type from Reid, Hawley & Gizis (1995a).
MB89: radial velocity from Marcy & Benitz (1989).
D98: radial velocity from Delfosse et al. (1998).

Table 3. Radial velocity measurements.

Star	$\langle V\rangle$ km s^{-1}	σ_V km s^{-1}	ΔV_{WD} km s^{-1}	V_{hel} km s^{-1}	Star	$\langle V\rangle$ km s^{-1}	σ_V km s^{-1}	ΔV_{WD} km s^{-1}	V_{hel} km s^{-1}
		1997 January	field stars						
Gl 83.1	ref		0.57	−28.6	Gl 54.1	28.17	0.18	0.76	27.98
LP 771-95	−1.28	0.24	0.52	−1.23	LP 771−96AB	−5.67	0.30	0.38	−5.48
RHy 80	1.67	0.45	−0.11	2.35	RHy 110	59.26	0.24	−0.84	60.67
RHy 254	−4.49	0.40	0.20	−4.12					
		1997 January	Hyads						
RHy 9	36.82	0.28	0.41	36.98	RHy 23	36.19	0.25	0.33	36.43
RHy 42A	30.28	0.74	0.09	30.76	RHy 46	36.45	0.33	0.05	36.97
RHy 42B	41.70	0.81	0.09	42.18					
RHy 49	36.41	3.40	−0.25	37.22	RHy 60	36.33	0.78	−0.10	37.00
RHy 64	35.71	0.86	−0.23	36.51	RHy 88A	38.50	0.27	0.00	39.07
RHy 88B	33.82	0.19	−0.15	35.04	RHy 98	38.13	3.56	−0.48	39.19
RHy 101	37.37	0.98	−0.28	38.22	RHy 115	38.21	0.28	−0.13	38.91
RHy 119	36.70	0.41	−0.32	37.59	RHy 126	36.18	2.61	−0.54	37.29
RHy 129	38.12	0.20	−0.37	39.06	RHy 143	37.62	0.28	−0.43	38.62
RHy 158	38.77	0.38	−0.51	39.85	RHy 163	36.70	7.41	−0.82	38.09
RHy 244	38.13	0.23	0.74	37.96	RHy 260	40.32	0.24	0.30	40.59
RHy 297	39.83	0.74	0.11	40.29	RHy 298	40.25	0.26	0.19	40.43
RHy 301	39.73	0.95	−0.92	40.98	RHy 309	39.33	0.24	−0.92	40.82
		1997 December	field stars						
Gl 402	−4.68	0.25	−2.81	−1.10	Gl 445	−113.28	0.26	−1.01	−111.50
Gl 447	−33.55	0.24	−1.60	−31.18	Gl 876	−3.74	0.20	−1.13	−1.97
RHy 110	56.11	0.09	−3.24	60.12	Gl 234A	ref		0.77	14.85
		1997 December	Hyads						
RHy 9	33.03	0.25	−3.37	37.17	RHy 23	32.35	0.29	−3.33	36.45
RHy 42A	14.96	1.01	−3.15	18.88	RHy 46	32.68	0.36	−3.46	36.91
RHy 42B	53.67	0.53	−3.15	57.59					
RHy 60	32.31	0.78	−3.61	36.69	RHy 64	31.83	0.87	−3.49	36.09
RHy 83	33.27	0.45	−3.62	37.66	RHy 88A	35.05	0.35	−3.30	39.13
RHy 88B	32.18	0.24	−3.18	36.13	RHy 98	32.73	1.65	−3.29	36.89
RHy 101	33.32	0.41	−3.65	37.74	RHy 115	34.66	0.39	−3.63	39.06
RHy 119	33.91	0.37	−3.01	37.69	RHy 129	34.96	0.39	−3.19	38.92
RHy 143	34.43	0.40	−3.31	38.51	RHy 158	33.55	0.37	−3.31	37.63
RHy 162	34.28	2.48	−2.84	37.89	RHy 163	34.82	0.70	−2.87	38.46
RHy 182	35.52	0.39	−2.98	39.27	RHy 199	35.20	0.71	−2.84	38.81
RHy 200	36.27	0.52	−2.79	39.83	RHy 202	35.19	0.38	−2.75	38.71
RHy 219	35.87	0.54	−2.63	39.27	RHy 221	37.08	0.33	−2.70	40.55
RHy 225	36.91	0.31	−2.57	40.25	RHy 231	35.68	0.42	−2.65	39.10
RHy 230	37.40	1.38	−1.51	39.68	RHy 240A	37.59	1.34	−1.37	39.73
RHy 240B	36.22	0.21	−1.24	38.33	RHy 260	38.73	0.25	−1.08	40.68
RHy 281	31.26	1.32	−1.29	33.32	RHy 297	38.42	0.54	−1.14	40.33
RHy 301	38.27	0.54	−1.04	40.08	RHy 331	38.23	0.30	−1.13	40.13
RHy 346	39.00	0.20	−1.10	40.90	RHy 367	39.18	0.20	−1.15	41.10
RHy 371	36.37	0.67	−1.09	38.23	RHy 377	40.65	0.47	−0.98	42.40
G 8-17	34.96	0.22	−1.12	36.85	RHy 386	39.41	0.51	−1.10	41.30
RHy 391	37.88	0.82	−1.04	39.69	RHy 399	38.97	0.25	−1.02	40.76
RHy 402	39.23	0.52	−0.92	40.92	RHy 403	41.22	0.47	−0.97	42.96
RHy 165	36.82	2.10	−0.92	38.51	RHy 390	39.12	1.63	−1.05	40.94
RHy 242	39.22	0.41	−0.46	40.45	RHy 132	37.56	0.41	−0.50	38.83
RHy 376	39.90	0.32	−0.33	41.00	RHy 83	36.79	0.52	−0.28	37.84
RHy 46	35.58	0.26	−0.54	36.89	RHy 46	35.61	0.29	−0.35	36.73
RHy 46	35.73	0.32	−0.41	36.91	RHy 230	38.46	1.59	−0.57	39.80
RHy 281	30.97	1.07	−1.06	32.80	RHy 297	38.42	0.39	−1.22	40.41
RHy 386	39.60	0.79	−1.21	41.58	RHy 402	38.95	0.78	−1.25	40.97
RHy 403	71.41	0.74	−1.58	73.76					
		1999 December	field stars						
Gl 83.1	ref		0.71	−28.6	Gl 447	−30.63	0.32	1.57	−31.49
Gl 234A	16.35	0.12	0.18	16.17	Gl 447	−30.90	0.15	−31.21	0.31
		1999 December	Hyads						
RHy 42	36.31	0.16	0.95	36.07	RHy 281	32.37	1.19	0.42	32.66
RHy 403	69.01	0.56	0.29	69.42	RHy 42	35.88	0.25	0.0	36.59
RHy 403	74.68	0.42	−0.02	75.41	RHy 42	36.18	0.33	−0.15	37.04
RHy 403	78.02	0.34	−0.10	78.83	RHy 42	36.23	0.28	0.48	33.19
RHy 281	32.36	0.51	−0.21	33.19	RHy 403	79.24	−0.04	79.99	
RHy 42	36.10	0.31	0.42	36.39	RHy 403	78.49	0.40	0.74	78.46
RHy 42	36.74	0.27	0.44	37.01	RHy 403	75.24	0.64	0.80	75.15
RHy 42	37.08	0.31	0.72	37.07	RHy 403	72.48	0.44	1.03	72.16
RHy 342	36.79	0.16	0.04	36.75	RHy 403	20.27	0.46	0.04	20.23
RHy 42	35.66	0.57	0.07	35.59	RHy 403	27.72	0.64	0.03	27.69
RHy 42	36.39	0.11	−0.46	36.85	RHy 403	36.80	0.37	−0.40	37.20

Table 3 – *continued*

Star	$\langle V \rangle$ km s^{-1}	σ_V km s^{-1}	ΔV_{WD} km s^{-1}	V_{hel} km s^{-1}	Star	$\langle V \rangle$ km s^{-1}	σ_V km s^{-1}	ΔV_{WD} km s^{-1}	V_{hel} km s^{-1}
RHy 42	36.24	0.17	−0.35	36.59	RHy 281	32.02	1.19	−0.75	32.77
RHy 403	46.33	0.57	−0.71	47.04	RHy 42	35.92	0.28	−0.43	36.35
RHy 403	56.50	0.35	−0.23	56.73	RHy 42	36.17	0.35	−0.42	36.59
RHy 403	63.94	0.33	−0.19	64.13					

determined from thorium-argon lamp exposures made at the start of each night, using standard IRAF routines to apply that calibration to the individual observations. Previous experience has shown that this technique provides velocities accurate to $\pm 1\,\mathrm{km\,s^{-1}}$. Interspersing calibration arcs between programme observations does not necessarily lead to an improvement in the stability of the wavelength scale. However, other means are available to establish the velocity zero-point with higher accuracy, as described in the following section. We have not attempted to set any of the spectra on an absolute flux scale.

3 RADIAL VELOCITY AND STELLAR ROTATION MEASUREMENTS

The primary aim of this programme is to identify spectroscopic binaries in the Hyades cluster. In general, achieving such a goal demands multiple, high-accuracy spectroscopic observations: our initial reductions provide velocities accurate only to $\pm 1\,\mathrm{km\,s^{-1}}$, and we have only one observation of almost half of the stars listed in Table 1. As discussed further below, we have been able to refine the accuracy of our velocity determinations. Moreover, we can utilize even single observations for binary detection, since we have the advantage of targetting stars with known space motion.

The standard method of determining radial velocities is cross-correlation of the calibrated spectra against data for a standard star of similar spectral type and known radial velocity (Tonry & Davis 1979). Uncertainties in the derived velocities depend both on random errors, which can be estimated from the width of the cross-correlation peak and interorder agreement in the derived velocities, and on the accuracy of the wavelength calibration. In past observations, we have noted systematic differences of 1 to $1.5\,\mathrm{km\,s^{-1}}$ in repeated HIRES obervations of individual stars. These offsets are present in both sky and stellar spectra, even if calibrated using adjacent Th-Ar arcs. The discrepancies may originate either through differences in the illumination of the slit, or through internal variations in the optical elements within the HIRES instrument.

Given those concerns, we adopt a two-stage approach to determining heliocentric velocities. First, the observations are cross-correlated against standard stars in the usual manner; second, we use terrestial features in the stellar spectra to set the observations on a uniform zero-point.

3.1 Relative velocity determination

In cross-correlation, the spectral type of the standard template must be a good match to that of the programme stars. For the current observations, the two field stars which best satisfy this constraint are the M4.5 dwarfs Gl 83.1 (1997 January and 1999 December) and Gl 234A (1997 December). Neither has published high-precision velocity measurements: heliocentric velocities for both systems have been measured by Delfosse et al. (1998), but the results are cited only to the nearest $\mathrm{km\,s^{-1}}$. Moreover, Gl 234A is the primary component in a wide binary, with $a \sim 4.17$ au, $P \sim 16.60$ yr, $M_2/M_1 \sim 0.5$ (Henry & McCarthy 1993).

Table 4. Comparison with previous observations: Hyades stars.

Star	V_{hel} this paper	$v \sin(i)$	V_{hel} other	$v \sin(i)$	reference
RHy 143	38.6	4	37.5	6.5	Stauffer et al. 1997
RHy 225	40.3	<2.5	39.2	<6	
RHy 386	41.5	9	41.1	11	Jones et al. 1996
RHy 23	36.4	4	36.3	6.5	Terndrup et al. 2000
RHy 60	36.85	19	37	19	
RHy 115	38.9	7	39.0	9	
RHy 119	37.6	9	37.1	9	
RHy 158	37.6/39.5	11	40.9	11	
RHy 202	38.7	2.5	38.8	<5	
RHy 240b	38.2	14.5	40.5	14.5	
RHy 346	40.9	3.5	41.1	6	
RHy 386	41.5	9	41.9	11.5	
RHy 390	40.9	18	40.5	18	

We have therefore determined heliocentric velocities for both of our template stars by cross-correlation against our data for field M dwarfs observed by Marcy & Benitz (1989): Gl 402, 447 and 876. Marcy & Benitz also observed Gl 831, but at only one epoch. Since that star is known to be a binary, it is not included in our zero-point determination. Table 2 lists the results for all of the field stars. We derive a heliocentric velocity of $-28.6\,\mathrm{km\,s^{-1}}$ for Gl 83.1, with no significant variation evident in our three observations. In contrast, Gl 234A has a heliocentric velocity of $14.85\,\mathrm{km\,s^{-1}}$ in 1997 December, while we measure $16.17\,\mathrm{km\,s^{-1}}$ in 1999 December.

The individual spectra were cross-correlated, order by order, against the appropriate template using the IRAF routine *fxcor*. The velocity differences computed by this routine include heliocentric corrections. Three echelle orders are dominated by terrestial features: 6800–6890 Å, the B-band; 7520–7630 Å, the A-band; and 8220–8330 Å. We excluded those orders when determining the mean velocity measured for the programme stars. In most cases, the remaining orders correlate well, with cross-correlation peaks of amplitude 0.7–0.9 and formal uncertainties of 0.3 to $0.7\,\mathrm{km\,s^{-1}}$ in the individual velocity measurements. We have averaged the latter measurements to derive the radial velocities, $\langle V \rangle$ listed in Tables 3 and 4, citing the rms dispersion about the mean, σ_V, as an estimate of the uncertainty. In most cases, the latter values are 0.15 to $0.3\,\mathrm{km\,s^{-1}}$. Approximately 20 per cent of the sample have substantial rotational velocities, $v \sin(i) > 15\,\mathrm{km\,s^{-1}}$. These stars have higher uncertainties in the derived velocities.

3.2 Establishing the velocity zero-point

The optimum method of wavelength calibration is to obtain a calibration spectrum simultaneously with the programme star

data. Current surveys for extrasolar planets, which require accuracies exceeding $10\,\mathrm{m\,s^{-1}}$, achieve this goal by inserting an iodide cell below the slit, superimposing iodine absorption lines on the stellar spectrum (Marcy & Butler 1992). Unfortunately, the Hyades M dwarfs are too faint to permit use of this technique. However, the Earth's atmosphere provides a ready-made reference frame, superimposing a grid of O_2 and OH lines on each stellar spectrum. Observations have shown that the wavelengths of these lines are stable to $\sim 40\,\mathrm{m\,s^{-1}}$, insufficient for extrasolar-planet searches, but more than adequate for current purposes.

The terrestial atmosphere supplies both emission and absorption lines. Of these two options, the latter is preferable for calibration purposes, since, as with the iodide cell, the optical path followed by the calibration spectrum is, perforce, identical to the stellar spectrum. In principle, we could estimate the drift in zero-point using the Hyades/Gl 83.1/Gl 234A cross-correlation results for orders dominated by terrestial absorption. However, stellar features weaken the correlation. We therefore use white dwarf stars as our terrestial templates.

G74-7, our 1997 January template, is a DAZ white dwarf, with strong Ca II H and K absorption; HS 0507A, used for our 1997 December observations, is the brighter of a pair of DA white dwarfs detected in the course of the Hamburg Schmidt quasar survey (Hagen et al. 1995); and 40 Eridani B, 1999 December, is the brightest accessible DA white dwarf. With the exception of broad Hα lines, the intrinsic spectrum is a featureless continuum at red wavelengths; all absorption features are due to the Earth's atmosphere. These stars provide excellent templates for calibrating zero-point drift of the wavelength scale.

Cross-correlating the programme stars against white dwarf spectra produces strong correlations in the orders which include the O_2 A- and B-bands. Fig. 1 compares the derived offsets from our January observations against the drift in velocity measured using the emission-line sky spectrum from the same observations. The agreement between the two independent measurements is good, with

$$V_{\mathrm{B\text{-}band}} - V_{\mathrm{em}} = 0.21 \pm 0.34\,\mathrm{km\,s^{-1}}$$

and

$$V_{\mathrm{A\text{-}band}} - V_{\mathrm{em}} = 0.10 \pm 0.19\,\mathrm{km\,s^{-1}}.$$

The amplitude of variation, $\pm 1\,\mathrm{km\,s^{-1}}$, is typical for a single night. Given these results, we have combined the A- and B-band measurements, giving the former twice the weight of the latter, to derive the appropriate correction. Those values are listed in Table 3 as ΔV_{WD}, and the corrected, heliocentric velocities are listed as V_{hel}.

Table 4 compares our heliocentric velocity determinations against previously published results. Setting aside RHy 158, for reasons discussed in the following section, the mean residual, in the sense of the current measurements *minus* literature data, is

$$\Delta V_{R-O} = 0.04 \pm 0.88\,\mathrm{km\,s^{-1}}, \quad 12 \text{ stars}.$$

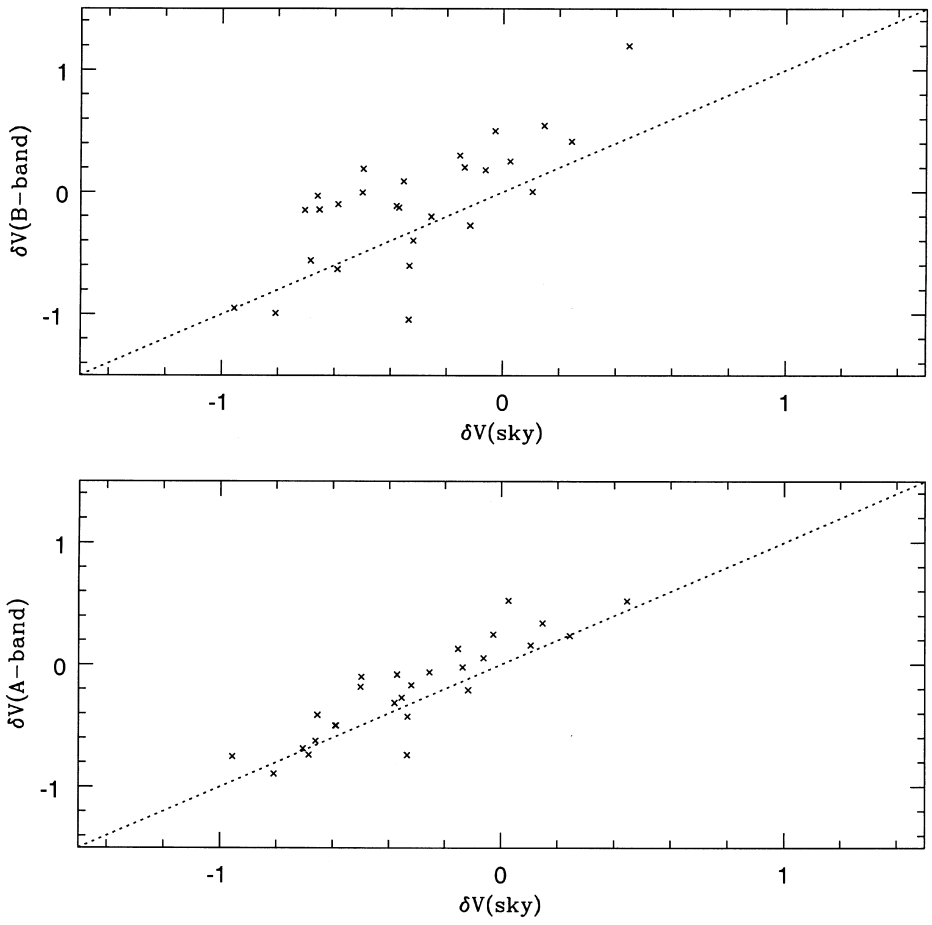

Figure 1. Comparison between velocity offsets for individual spectra derived by cross-correlation using atmospheric emission lines (abscissa) and the A- and B-band absorption features. Data are plotted from 1997 January, using G74-7 as the white dwarf template.

3.3 Rotation

Tonry & Davis (1979) originally demonstrated that the width of the peak in the cross-correlation function is dependent on the line profiles of both template and programme object. In extragalactic astronomy, this property is used to measure velocity dispersion; in stellar astronomy, rotation is usually the dominant contributor to line profile broadening. We have used this technique to estimate rotational velocities for the stars in our sample.

The relation between the measured width of the cross-correlation peak, fitted either with a Gaussian or parabolic profile, and $v\sin(i)$, the projected stellar rotation, is determined using spectra of a slowly rotating star which have been broadened artificially to match known rotational velocities. Cross-correlating those spectra against a template, also with known low rotation and of similar spectral type, provides the necessary calibration. We have used our observations of Gl 447 (rotation star) and Gl 402 (template) to calibrate our data. Both stars have negligible rotation, $v\sin(i) < 2.0\,\mathrm{km\,s^{-1}}$ and $<2.3\,\mathrm{km\,s^{-1}}$ respectively (Delfosse et al. 1998), and both are well matched in spectral type to the Hyades programme stars.

We chose two orders, $\lambda\lambda 7360$–7460 Å and $\lambda\lambda 7840$–7960 Å, for these measurements, avoiding both TiO bandheads and the stronger terrestial features. The Gl 447 spectrum was broadened following Gray's (1976) prescription. The HIRES data have a resolution of $R \sim 45\,000$, corresponding to a velocity of $v_{\mathrm{FWHM}} = 6.67\,\mathrm{km\,s^{-1}}$. This sets a lower detection limit of $v\sin(i) \sim 2.5\,\mathrm{km\,s^{-1}}$ for our rotation measurements. Results for the full sample of Hyades stars are tabulated and discussed in Section 5. Table 4 includes a comparison of our measurements against previously published results. We derive slightly lower rotational velocities for the slow rotators. However, the agreement is excellent for moderately and rapidly rotation stars.

4 IDENTIFYING SPECTROSCOPIC BINARIES

The conventional method of identifying spectroscopic binaries is to compare velocity measurements obtained at different epochs. Table 5 lists the relevant data from our observations, including both V_{hel} and the Modified Julian Date for each observaton. Almost half of the sample have only a single observation, but even those observations can be used to identify candidate spectroscopic binaries, since our targets are members of the Hyades cluster.

Perryman et al. (1998) have used astrometric data from the *Hipparcos* satellite and CORAVEL radial velocity observations to determine the mean distance of Hyades cluster members (46.34 ± 0.27 pc) and the cluster space motion ($45.72\,\mathrm{km\,s^{-1}}$). As noted above, those parameters correspond to a distance scale shorter by $\sim$5 per cent than that adopted in Reid (1993). In traditional open cluster analyses, absolute proper motion measurements are used to determine the location in (α,δ) of the convergent point. Given a known space motion for the cluster, the radial velocity of an idealized cluster member, $V_{\mathrm{rad}}^{\mathrm{P}}$, depends only on the angular distance from the convergent point, λ_{CP}. Similarly, the proper motion of a cluster members depends on both λ_{CP} and distance, allowing distance estimates to individual cluster members (Table 1).

Circumstances are more complicated for a relatively old cluster, such as the Hyades. As Perryman et al. (1988) point out, the velocity dispersion of $\sigma \sim 0.2\,\mathrm{km\,s^{-1}}$ leads to an intrinsic fuzziness in the convergent 'point'. Thus, when we invert the process, and predict V_{rad} based on an idealized convergent point, those predictions are uncertain by $\pm 0.2\,\mathrm{km\,s^{-1}}$. Indeed, since the Hyades is sufficiently old to have undergone significant mass segregation, the velocity dispersion (and corresponding uncertainty in $V_{\mathrm{rad}}^{\mathrm{P}}$) may be as high as 0.3–$0.4\,\mathrm{km\,s^{-1}}$ for low-mass stars. None the less, taking into account these uncertainties, a significant difference between the observed velocity and the expected velocity indicates either binary motion, or non-membership of the cluster. In the case of Hyades M dwarfs, chromospheric activity provides a means of deciding between those alternatives.

We have adopted the convergent point determined by Perryman et al. (1988) from their maximum-likelihood analysis: they derive $(\alpha = 96\overset{\circ}{.}5,\ \delta = 5\overset{\circ}{.}8)$ from a sample of 148 Hyades members. We also use their estimate of the Hyades space motion, $V = 45.72\,\mathrm{km\,s^{-1}}$. Table 5 lists both the expected radial velocity, V^{P}, for each Hyades star, and the observed–computed residual,

$$\delta V_{\mathrm{hel}}^{\mathrm{P}} = V_{\mathrm{hel}} - V^{\mathrm{P}}.$$

We note that the majority of the residuals are positive, with $\langle \delta V_{\mathrm{hel}}^{\mathrm{P}} \rangle = 0.64 \pm 0.68$ (excluding candidate binaries), suggesting that the kinematic model we have adopted for the cluster motion may require revision. The agreement is adequate for current purposes.

In order to assess the significance of differences between the predicted and observed velocities, we need to determine the uncertainty, ϵ_V, associated with $\delta V_{\mathrm{hel}}^{\mathrm{P}}$. These uncertainties stem from two sources: empirical measuring accuracy, and intrinsic dispersion in cluster motions. Our data provide several means of estimating the former:

(1) five observations in 1997 of RHy 46 give $\langle V_{\mathrm{hel}} \rangle = 36.88 \pm 0.09\,\mathrm{km\,s^{-1}}$;

(2) 13 observations (1999 December) of RHy 42 give $\langle V_{\mathrm{hel}} \rangle = 36.57 \pm 0.42\,\mathrm{km\,s^{-1}}$;

(3) five observations (1997–1999) of RHy 281 give $\langle V_{\mathrm{hel}} \rangle = 32.95 \pm 0.29\,\mathrm{km\,s^{-1}}$, and

(4) 21 repeat observations of 20 stars with $|\Delta V_{\mathrm{epoch}}| < 1\,\mathrm{km\,s^{-1}}$ give a mean difference of $-0.115 \pm 0.34\,\mathrm{km\,s^{-1}}$.

On that basis, we estimate that an rms uncertainty of $0.35\,\mathrm{km\,s^{-1}}$ is appropriate for the heliocentric velocity measurements given in Table 3. If we assume that the intrinsic velocity dispersion of Hyades M dwarfs has a similar value, then we derive a minimum value of $\epsilon_V = 0.5\,\mathrm{km\,s^{-1}}$. If σ_V, the order-to-order rms dispersion of velocity measurements for a given observation, exceeds $0.5\,\mathrm{km\,s^{-1}}$ (Table 3), then we let $\epsilon_V = \sigma_V$. Column 7 in Table 5 gives the ratio of $\delta V_{\mathrm{hel}}^{\mathrm{P}}$ to ϵ_V for each star.

5 DISCUSSION

5.1 New spectroscopic binaries

Fig. 2 plots the colour–magnitude diagram for lower main-sequence in the Hyades, marking the spectroscopic binaries and candidate binaries identified from our observations. Three stars in Table 5 are prime binary candidates: RHy 42, 281 and 403. Two are confirmed as binaries based on the 1997 data alone: RHy 42, a double-lined system; and RHy 403, a single-lined system, whose radial velocity increased by $31\,\mathrm{km\,s^{-1}}$ in only 26 hours in 1997 December. The third star, RHy 281, exhibits no variation in velocity, but the measured value is offset by $\sim 5\sigma$ from the expected value for a cluster member. These three stars were therefore chosen as the focus of our most recent observations.

Table 5. Heliocentric velocities.

Rhy	MJD 50000+	V_{hel} km s^{-1}	ϵ_V km s^{-1}	V^P km s^{-1}	δV^P_{hel} km s^{-1}	$\delta V/\epsilon_V$	ΔV_{epoch} km s^{-1}	Hα EW Å
9	460.31252	36.98	0.5	36.12	0.86	1.7		5.1
	792.24254	37.22	0.5		1.1	2.2	0.24	3.8
23	460.32099	36.42	0.5	35.70	0.72	1.4		3.4
	792.25098	36.50	0.5		0.8	1.6	0.08	4.4
42	460.32924	A 30.77	0.7	36.19				3.4
		B 42.18	0.8		0.28	0.4		
	792.25906	A 18.88	0.6					4.3
		B 57.59	0.5		2.0	4		
	1541.18103	36.07	0.5		−0.12	−0.2		3.5
	1541.23980	36.59	0.5		0.40	0.8		4.0
	1541.29145	37.04	0.5		0.75	1.5		3.8
	1541.33793	36.46	0.5		0.27	0.5		3.8
	1541.40453	36.39	0.5		0.20	0.4		3.7
	1541.44922	37.01	0.5		0.82	1.6		3.5
	1541.47928	37.07	0.5		0.86	1.7		3.9
	1542.18976	36.75	0.5		0.56	1.1		4.7
	1542.24088	35.59	0.5		−0.60	1.2		4.9
	1542.28896	36.85	0.5		0.66	1.3		5.6
	1542.33138	36.59	0.5		0.40	0.8		4.7
	1542.38990	36.35	0.5		0.16	0.3		4.6
	1542.43474	36.59	0.5		0.40	0.8		4.7
46	460.34582	36.97	0.5	36.19	0.78	1.6		3.8
	792.31009	36.91	0.5		0.72	1.4	−0.06	3.9
	794.39999	36.90	0.5		0.73	1.4	−0.07	4.1
	794.40812	36.73	0.5		0.54	1.1	−0.24	4.2
	794.41615	36.91	0.5		0.72	1.4	−0.06	4.2
49^r	460.34517	37.22	3.4	36.02	1.2	0.4		4.8
	792.31824	34.75	2.0		−1.27	−0.7	−2.47	4.4
60	460.36269	37.00	0.8	36.43	0.57	0.7		3.1
	792.32645	36.70	0.8		0.27	0.3	−0.3	3.9
64	460.37087	36.23	0.9	36.33	−0.1	−0.1		3.2
	792.33456	36.09	0.7		−0.24	−0.3	−0.14	3.4
83	792.35098	37.66	0.5	37.14	0.52	1.0		4.8
	794.42461	37.84	0.5		0.70	1.4	0.18	3.9
88A	460.39414	39.07	0.5	36.61	2.46	4.9		0.5a
	792.35970	39.13	0.5		2.52	5.0	0.06	0.5a
88B	460.40029	35.04	0.5	36.61	−1.57	−3.2		2.8
	792.36787	36.13	0.5		−0.48	1.0	1.09	1.4
98^r	460.40542	39.19	3.6	36.77	2.42	0.7		5.0
	792.37262	36.91	1.65		0.14	0.1	−2.28	3.7
101	460.41391	38.22	1.0	37.85	0.37	0.4		4.3
	792.38320	37.74	0.5		−0.11	−0.2	−0.48	4.4
115	460.43029	38.91	0.5	37.32	1.59	3.2		3.6
	792.40683	39.06	0.5		1.74	3.5	0.17	3.5
119	460.43856	37.59	0.5	37.14	0.45	0.9		4.4
	792.41942	37.68	0.5		0.54	1.1	0.09	4.0
126^r	460.44699	37.29	2.6	37.76	−0.47	−0.2		6.0
129	460.45539	39.06	0.5	38.04	1.02	2		3.6
	792.42803	38.92	0.5		0.88	1.8	−0.14	4.0
132	793.50806	38.83	0.5	37.81	1.02	2.0		4.3
143	460.46358	38.62	0.5	37.89	0.73	1.5		3.0
	792.43758	38.51	0.5		0.62	1.2	−0.11	6.6
158	460.47216	39.45	0.5	38.71	0.74	1.5		4.1
	792.44589	37.63	0.5		−1.08	−2.2	−1.82	4.2
162^r	460.48031	38.09	5.0	37.83	0.26	0.05		4.7
	792.47709	37.87	2.5		0.04	0	−0.22	5.3
163	792.48866	38.46	0.7	38.30	0.16	0.2		3.2
165^r	793.47003	38.51	2.1	37.82	0.69	0.3		7.7
165^r	793.47003	38.51	2.1	37.82	0.69	0.3		7.7
182	792.49718	39.27	0.5	38.59	0.68	1.4		4.0
199	792.50523	38.81	0.7	38.26	0.55	0.7		4.1
200	792.51342	39.83	0.5	39.00	0.83	1.6		3.6
202	792.52180	38.71	0.5	38.31	0.4	0.8		3.0
219	792.52990	39.27	0.5	38.73	0.54	1.1		4.3
221	792.53800	40.55	0.5	38.63	1.92	3.8		2.9
230	793.24775	39.68	1.4	38.74	0.94	0.7		5.2
	794.44496	39.80	1.6		1.06	0.7	0.12	4.2
231	792.55084	39.10	0.5	38.63	0.47	0.9		5.8
240A	793.26704	39.73	1.3	38.90	0.83	0.6		6.0
240B	793.27862	38.23	0.5	38.90	−0.67	1.3		4.0

Table 5 – *continued*

Rhy	MJD 50000+	V_{hel} km s^{-1}	ϵ_V km s^{-1}	V^P km s^{-1}	δV^P_{hel} km s^{-1}	$\delta V/\epsilon_V$	ΔV_{epoch} km s^{-1}	Hα EW Å
242	793.50000	40.45	0.5	39.16	1.26	2.5		3.1
244	460.24334	37.96	0.5	38.54	−0.58	−1.2		4.7
260	460.26471	40.59	0.5	39.28	1.31	2.6		3.6
	793.28678	40.58	0.5		1.30	2.6	−0.01	4.3
281	793.29503	33.32	1.3	39.22	−5.80	−4.5		4.6
	794.45771	32.80	1.1		−6.42	−5.8	−0.52	22.8
	1541.18724	32.66	1.2		−6.56	−5.5	−0.66	6.7
	1541.34444	33.19	0.6		−6.03	−10.1	−0.13	6.1
	1542.33699	32.77	1.2		−6.45	−5.4	−0.55	5.5
297	460.27310	40.29	0.5	39.66	0.63	1.3		4.1
	793.30331	40.33	0.5		0.67	1.3	0.04	4.7
	794.49131	40.41	0.5		0.75	1.5	0.12	4.3
298	460.28963	40.63	0.5	39.68	1.05	2.1		3.3
	793.31490	40.61	0.5		1.03	2.1	−0.02	4.1
301	460.48851	40.98	1.0	39.77	1.2	1.2		5.0
	793.32307	40.08	0.5		0.31	0.6	−0.9	6.1
309	460.49697	40.82	0.5	39.15	1.67	3.1		4.9
331	793.33144	40.13	0.5	39.28	0.85	1.7		3.0
346	793.34021	40.90	0.5	40.16	0.74	1.5		3.5
367	793.34828	41.10	0.5	40.24	0.86	1.7		4.8
369	793.35632	41.51	0.5	40.30	1.21	2.4		2.7
371	793.36490	38.23	0.7	39.82	−1.59	−2.3		3.8
376	793.51613	41.00	0.5	39.99	1.01	2.0		3.8
377	793.37344	42.40	0.5	40.38	2.02	4.0		3.8
386	793.40658	41.30	0.5	40.08	1.22	2.4		4.4
	794.50953	41.58	0.8		1.50	1.9	0.28	4.8
390	793.48502	40.94	1.6	39.84	1.10	0.7		8.7
391	793.42219	39.69	0.8	39.61	0.08	0.1		5.1
399	793.43026	40.76	0.5	39.90	0.86	1.7		3.8
402	793.43834	40.92	0.5	39.92	1.0	2.0		2.9
	794.53181	39.97	0.8		0.05	0	−0.95	3.8
403	793.45354	42.96	0.5	40.11	1.75	3.5		5.2
	794.54738	73.76	0.8		33.7	42	30.80	5.7
	1541.19393	69.42	0.6		29.3	49	26.46	7.8
	1541.24538	75.41	0.5		35.3	71	32.45	7.5
	1541.29500	78.83	0.5		38.7	77	35.87	6.2
	1541.35213	79.99	0.8		39.9	50	37.03	8.1
	1541.40799	78.46	0.5		38.4	77	35.50	6.4
	1541.45265	75.15	0.6		35.0	58	32.19	5.9
	1541.48272	72.16	0.5		32.1	64	29.20	3.9
	1542.19549	20.23	0.5		−19.8	−40	−22.69	7.0
	1542.24438	27.69	0.5		−12.4	−25	−15.27	5.9
	1542.29250	37.20	0.5		−2.91	−6	−5.76	7.2
	1542.34197	47.04	0.6		6.9	12	4.08	6.4
	1542.39357	56.73	0.5		16.6	33	13.77	6.2
	1542.43815	64.10	0.5		24.0	48	21.14	6.2
G8-17	793.39242	36.85	0.5	35.96	0.91	1.8		9.8

Stars identified with superscript^r have rotational velocities exceeding 15 km s^{-1}.

Fig. 3 plots the results of our 1999 December observations. RHy 403 is confirmed as a spectroscopic binary. The curve plotted is a simple sine-wave with a period of 1.276 d and an amplitude of 40 km s^{-1}, matched by eye to the data. Phase zero is at MJD = 51541.3521 d. The uncertainty in the derived period is ±0.005 d. The 1997 December observations are consistent with being obtained at phases of $\phi = 0.487$ and 0.339 respectively, with $\phi =$ 0.25 at 40794.429. The total number of cycles between the latter date and the observed maximum on December 29 can only be given as 584 ± 2.

The cross-correlation functions from our 1997 observations of RHy 42 clearly identify the star as a double-lined spectroscopic binary, as illustrated in Fig. 4. We also plot Hα emission-line data: the unusual profile in 1997 December is the result of the superposition of two lines of almost equal strength, each possessing a central reversal. The Ca I line at 6598 Å is also clearly double at the latter epoch. However, there is no evidence for either velocity variations or line-splitting in the 1999 December data. These observations are consistent with the identification of RHy 42 as a moderate-period binary system. The semi-major axis in an equal-mass binary is given by

$$a = \frac{\mathcal{G}(M_1 + M_2)}{v^2_{\rm circ}}.$$

Both components have $M_V \sim 12.5$, or, from Henry & McCarthy's (1993) mass–M_V relation, $M \sim 0.2\,M_\odot$. If we assume that the observed velocity difference in 1997 December, $\delta V = 34$ km s^{-1}, is close to the maximum value, and an inclination of 45°, then $v_{\rm circ} \sim 24$ km s^{-1} and $P \sim 0.75$ yr. Presumably our 1999 observations happened to catch the system at phase $\phi = 0°$ or 180°, with both stars having radial velocities close to the systemic value.

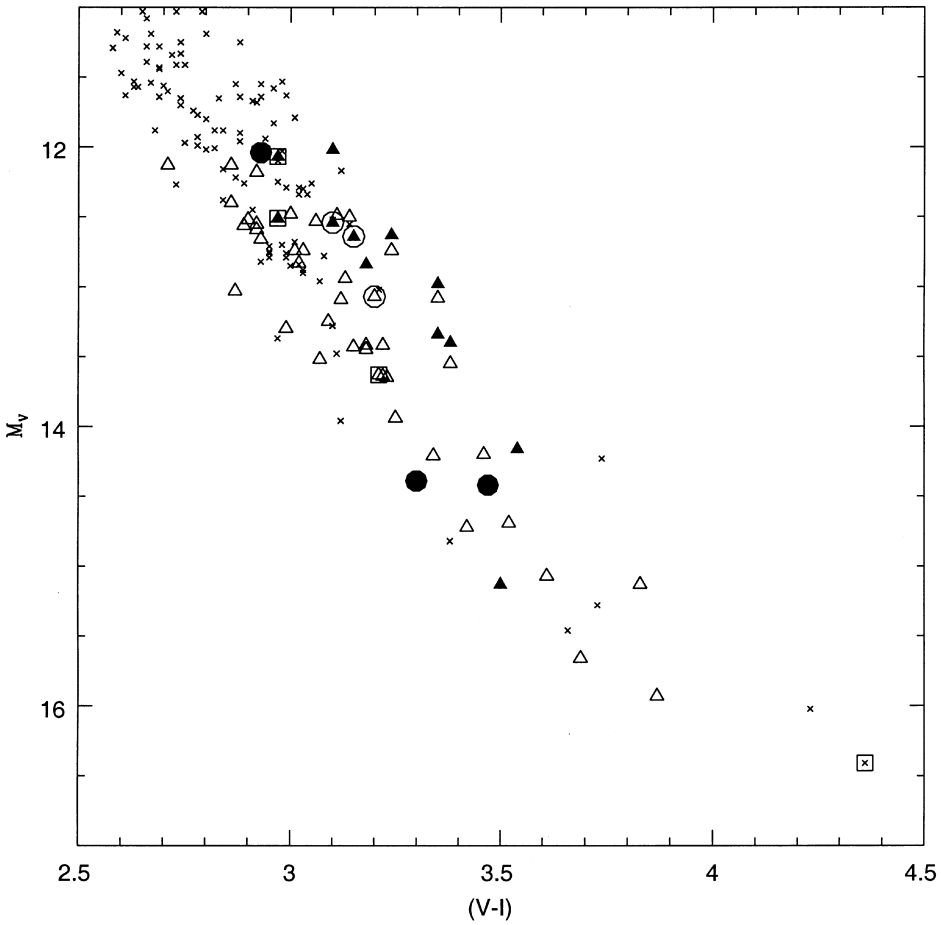

Figure 2. The $[M_V, (V-I)]$ colour–magnitude diagram for late-type Hyades dwarfs. Crosses are stars lacking *HST* observations; open triangles are stars unresolved by *HST* (RG97); solid triangles are resolved *HST* binaries (RG97); solid points mark the locations of RHy 42, 281 and 403; the three possible velocity variables, RHy 158, 221 and 377, are identified using open circles, while open squares identify four stars with unusual cross-correlation profiles: RHy 49, 244, 162 and 165.

Although RHy 281 has a radial velocity offset by 6 km s^{-1} from that expected for a Hyades star, our data show no evidence for significant velocity variation. The rms dispersion of all five observations, spanning two years, is only 0.29 km s^{-1}. The average Hα emission properties of this star are entirely consistent with Hyades membership. It is possible that RHy 281 may be no longer be bound to the Hyades cluster proper, though still part of the more extensive moving group. Alternatively, RHy 281 may be a long-period binary system, with an as-yet undetected low-mass companion. Further observations of this star are clearly warranted.

Seven other stars are identified as candidate binaries: three on the basis of the velocity data listed in Table 5; four display anomalies in the shape of the cross-correlation peak, with one star almost certainly binary. In the former group, RHy 221 and 377 both have only a single velocity determination, but in both cases, $\delta V/\epsilon_V \sim 4$. Both are known as a binary from *HST* observations. The peak in RHy 377's cross-correlation function is slightly asymmetric towards lower velocities, suggesting that the known companion may be responsible for the offset from the predicted velocity. The third star is RHy 158. Our two velocity determinations differ by only 1.8 km s^{-1} ($\sim 4\epsilon_V$), but this star was also observed by Terndrup et al. (2000). Their datum differs significantly from both our measurements.

RHy 49, 162, 165 and 244 all have cross-correlation functions with maxima suggestive of double-lined systems, with velocity separations of 5 to 10 km s^{-1} (Fig. 5). The first three stars are all rapid rotators, and it is possible that rapid rotation, rather than binarity, may be responsible for the anomalous structure (although RHy 49 is resolved as binary by *HST*). RHy 244, however, has low $v\sin(i)$, and the narrow cross-correlation peak has blueward asymmetry, suggesting a contribution from a lower luminosity companion (see, for comparison, figs 3 and 7 in Stauffer et al. 1997). We know from *HST* imaging that RHy 244 has a companion at $\Delta \sim 0.1$ arcsec, $\delta I \sim 1.1$ mag. The observed asymmetry is not inconsistent with the expected velocity difference of these known components.

5.2 The companion of RHy 403

Our observations of RHy 403 provide sufficient information to set firm constraints on the mass of the companion. If we assume a circular orbit, as suggested by the sine curve matched against the data in Fig. 3, then the observed maximum velocity (80 km s^{-1}) and $V^{\rm P} \sim 40$ km s^{-1} imply an orbital velocity, $v\sin(i) = 40$ km s^{-1}, and a projected semimajor axis, $a\sin(i) \sim 701\,000$ km, or 0.0047 au. The systemic mass function is given by

$$f(m) = \frac{M_2^3 \sin^3(i)}{(M_1 + M_2)^2} = \frac{[a\sin(i)]^3}{P^2},$$

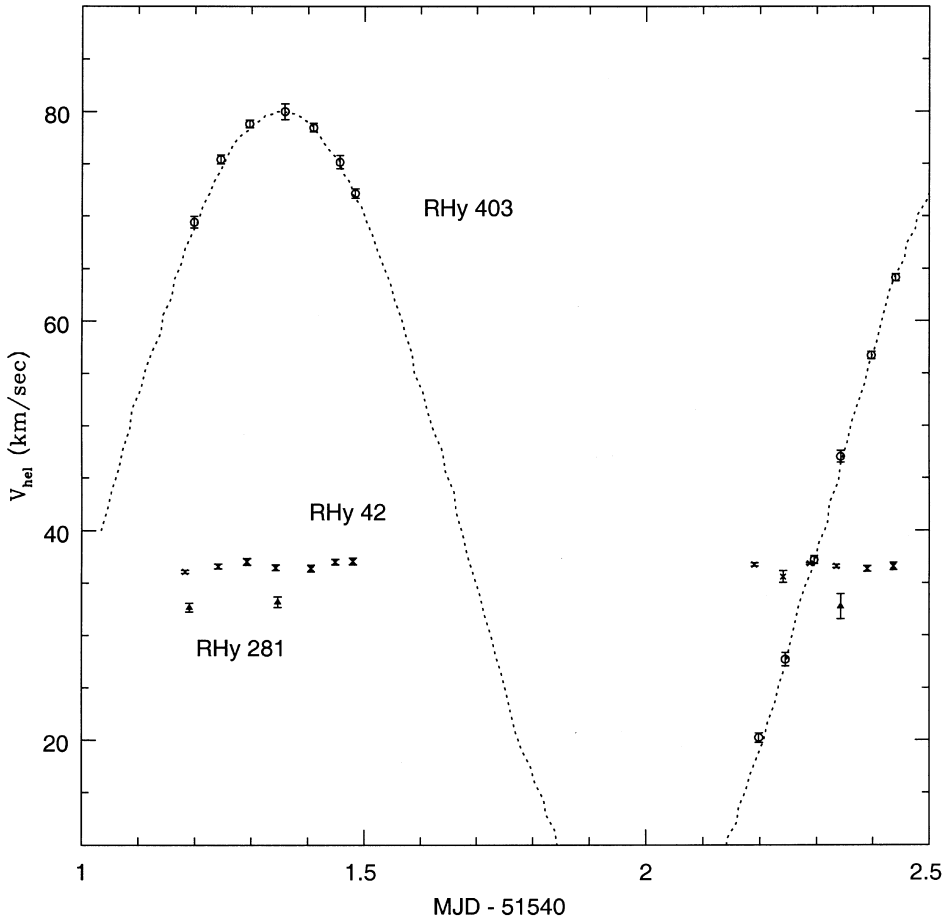

Figure 3. Velocity measurements from 1999 December for RHy 42 (crosses), RHy 281 (triangles) and RHy 403 (open circles). The curve matched to the last set of observations is a sine-wave with $P = 1.276$ d, amplitude $\pm 40\,\mathrm{km\,s^{-1}}$ and $T_0 = 51541.3521$ d (MJD).

where P is the period, 1.275 d. Substituting for P, we derive $f(m) = 0.0085$.

The fact that RHy 403 is a single-lined system allows us to estimate both a lower limit and an upper limit to M_2, the mass of the unseen companion. First, we can assume that the primary contributes most of the flux, even at 8000 Å. Hence the observed absolute magnitude provides an estimate of the mass of the primary, RHy 403A. Based on [BC_I, $(V-I)$ data from Leggett et al. (1996) and the photometry given in Table 1, we derive $M_{\rm bol} \sim 11$. Matched against the 600-Myr-old models computed by Burrows et al. (1993), this implies a mass of $\sim 0.15\,\mathrm{M}_\odot$. Substituting for M_1 in the mass function gives

$$M_2^3 \sin^3(i) = 1.9 \times 10^{-4} + 0.0085 M_2^2.$$

Setting $i = 90^\circ$ gives a lower limit to the mass of the companion, $M_2 > 0.062\,\mathrm{M}_\odot$, the first solution of the cubic equation.

In principle, RHy 403 could have an evolved companion; in practice, we can effectively rule out this option. With an age of 625 Myr, the lowest luminosity white dwarfs in the Hyades have $M_V \sim 12$ and $T_{\rm eff} \sim 15\,000$ K. Unresolved Hyades M dwarf/white dwarf binaries therefore have unusual colours, as demonstrated by HZ 9 [M2 + DA : $M_V = 10.6$, $(V-I) = 1.8$]. A neutron star companion, $M_2 = 1.4$ to $2\,\mathrm{M}_\odot$, requires $10^\circ.5 > i > 9.3$ and $0.026 < a < 0.029$ au; the extensive mass-loss during a supernova excludes the possibility of a primordial binary at these separations, while a system forming post-SN would still be expected to be bright at X-ray wavelengths. Stern et al. (1994) do not detect a *ROSAT* source close to RHy 403 in their survey of the cluster.

Given that the companion is either a low-luminosity main-sequence star or a brown dwarf, we can use the non-detection in both the direct spectrum and, more stringently, the cross-correlation analysis, to set an upper limit to M_2. A 0.06-$\mathrm{M}_\odot$ brown dwarf is predicted to have a temperature of $\sim$1900 K at age 625 Myr, corresponding to a spectral type of L2 and a luminosity of $10^{-4}\,\mathrm{L}_\odot$. With an absolute magnitude of $M_I \sim 15$, over 4 magnitudes fainter than RHy 403A, such an object lies well below our detection limit.

How faint a companion could we expect to detect? We can address this question in two ways. First, we have modelled an unequal-mass, late-type M-dwarf binary by combining appropriate spectra spanning a range of flux ratio. Based on those tests, we would expect to detect anomalies in the cross-correlation function for flux ratios exceeding 4:1 at $\lambda > 8000$ Å. Second, we can use observations of known spectroscopic binaries to infer detection limits. The data plotted in Fig. 5 suggest that we have detected RHy244B, $\delta I = 1.1$ mag, a flux ratio of $\sim$3:1. Similarly, Gl 831 is a known binary, with $M_V(\mathrm{A}) = 12.5$, $M_V(\mathrm{B}) = 15.5$; masses, $M_\mathrm{A} = 0.25\,\mathrm{M}_\odot$, $M_\mathrm{B} = 0.1\,\mathrm{M}_\odot$; $a \sim 0.21$ arcsec; and $P \sim 1.92$ yr (Henry 1990). Cross-correlating our spectra of Gl 831 against data for Gl 447 reveals an asymmetric peak (Fig. 6). Given $\Delta M_V \sim 3$ mag and $\Delta M_K \sim 1.3$ mag for the two components, the likely magnitude difference at I is close to 2 mag, or a flux ratio of $\sim$6:1.

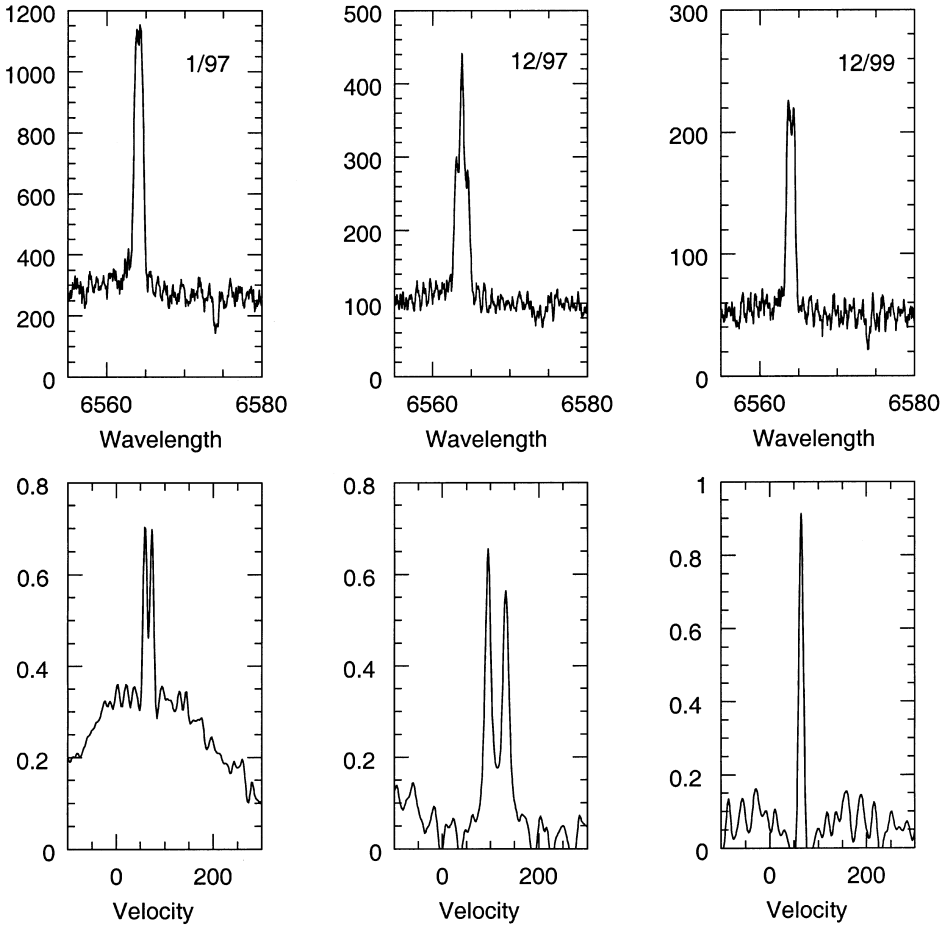

Figure 4. Hα emission and typical cross-correlation results for RHy 42 observations. The left-hand panels plot data from 1997 January; the middle panel, the 1997 December observation; the right-hand panel, data from 1999 December. The 1997 data clearly identify RHy 42 as a double-lined binary with components of nearly equal luminosity.

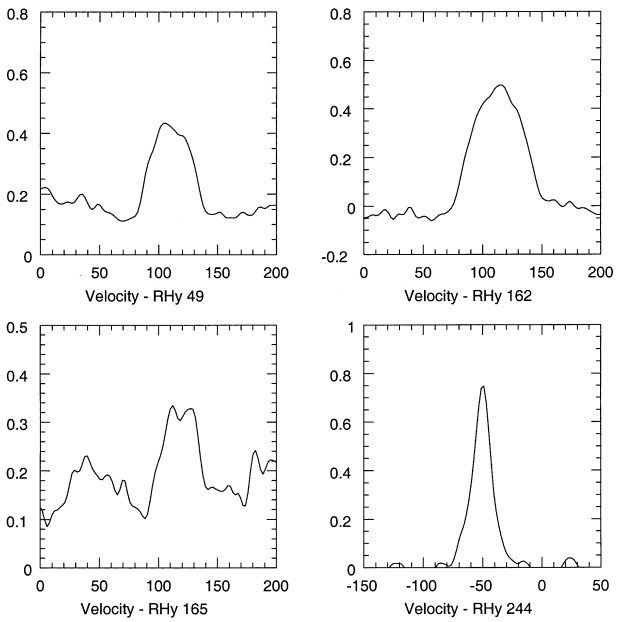

Figure 5. The central regions of the cross-correlation functions for RHy 49, 162, 165 and 244. The RHy 244 cross-correlation peak has an asymmetric blue wing, while the remaining three functions exhibit anomalous profiles.

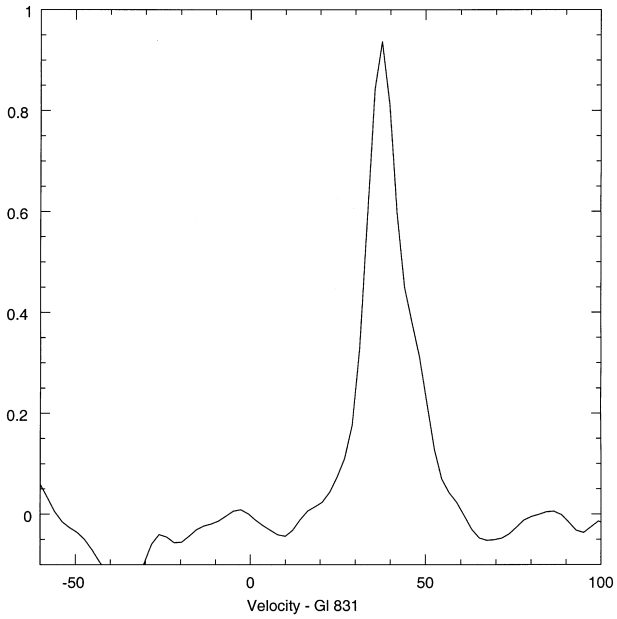

Figure 6. The cross-correlation peak for Gl 831AB matched against our template, Gl 447. The peak is asymmetric towards higher velocities. We interpret the asymmetry as due to the known companion, Gl 831B.

Table 6. Distribution of separations of binary components.

Δ	Hyades N	%	Field N	all M %	Field N	$M < 0.3\,M_\odot$ %
≤10 au	7	50%	17	50%	11	65%
10–100 au	5	36	11	32	6	35
>100 au	1	14	6	18	0	0

Our data for RHy 403 have lower signal to noise ratios, but it is unlikely that a companion with a flux ratio exceeding 4:1 would have escaped detection.

Our flux limit corresponds to an absolute magnitude of $M_I = 12.3$. Matched against the Burrows et al. (1993) models, this implies an upper mass limit of $M_2 < 0.095\,M_\odot$ for RHy 403B.

The lowest mass member of the Hyades currently known is LH0418+13 (Reid & Hawley 2000), with $M_I \sim 14$ and a mass of approximately $0.08\,M_\odot$. There is a probability of 72 per cent that the orbit of RHy 403B has $i > 50°$ and $M < 0.08\,M_\odot$; the probability is 66 per cent that $i > 55°$ and $M < 0.075\,M_\odot$. Thus RHy 403B is the first strong candidate for a brown dwarf member of the Hyades cluster. Unfortunately, since $a\sin(i) = 0.0047$ au and $r = 53$ pc, the maximum expected angular separation (for $M_2/M_1 \sim 2.5$) is only 0.25 mas. High-resolution spectroscopy at near-infrared wavelengths may provide stronger constraints on the upper mass limit.

5.3 The binary fraction of late-type Hyades M dwarfs

Prior to our observations, 10 of the 51 Hyades stars listed in Table 1 were known to be in binary systems. Our spectroscopic data add three definite new systems, RHy 42, 158 and 403, with RHy 281 also a strong candidate binary. In addition, RHy 162 and 165 show indications of duplicity, although the high intrinsic rotation of these stars render less certain the interpretation of the cross-correlation data. RHy 244, 377 and, perhaps, 49 are also possible spectroscopic binaries, but all three were identified previously as binaries based on the *HST* imaging. Our present radial velocity data are insufficient to determine whether the spatially resolved and hypothetical spectrscopic components are one and the same.

48 of the 51 M dwarfs listed in Table 1 have absolute magnitudes $M_V > 12$. Amongst the 47 systems (RHy 240A and B are observed separately) at least 11, and perhaps as many as 14, are binary or multiple systems – a multiplicity fraction of 23 to 30 per cent, with a formal uncertainty of 7 per cent. In comparison, the binary fraction amongst the (more completely surveyed) M dwarfs in the 8-pc sample is 33 per cent (Reid & Gizis 1997a).

Further analysis is limited by the small numbers in both the Hyades and field M dwarf samples. However, Table 6 compares the distribution of projected separations, Δ, adopting $\Delta = 0.8a$ for nearby systems with known orbits. We list statistics for all 8-pc binaries with M-dwarf primaries and for the subset where the primary has $M < 0.3\,M_\odot$. Within the admittedly large uncertainties, the field star and cluster distributions are identical.

6 CHROMOSPHERIC ACTIVITY IN LOW-MASS HYADES DWARFS

6.1 Rotation and activity

Table 8 lists the rotational velocities derived for the Hyades

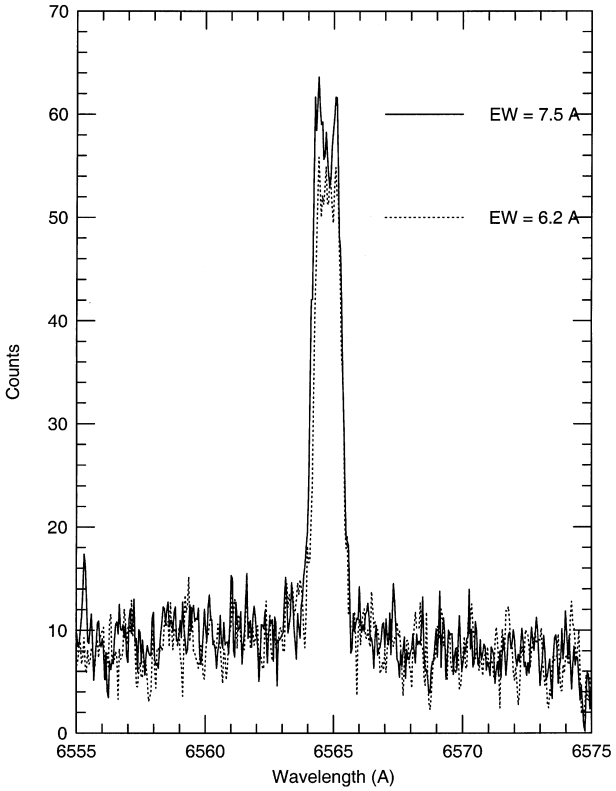

Figure 7. Hα line profiles from successive observations of RHy 403 (MJD 1541.245 and 1541.295).

dwarfs in our sample. All are chromospherically active, with substantial Hα emission. As indicated by the individual measurements listed in Table 5, the level of activity can vary by up to 30 per cent on relatively short time-scales. This intrinsic variability is the dominant source of uncertainty in determining stellar activity from one or two observations, as is the case here. Fig. 7 illustrates this effect, comparing successive observations of RHy 403 from 1999 December 29. Note the central reversal in the stronger Hα line profile. As Stauffer et al. (1997) point out, the majority of slow rotators [$v\sin(i) < 12\,\mathrm{km\,s^{-1}}$] have similar profiles, while stars with faster rotation have either flat-topped or peaked Hα lines.

We are interested in determining the extend of any correlation between the level of chromospheric activity and the underlying stellar rotation. The standard paradigm (Stauffer et al. 1997) envisages a direct correlation, with activity increasing with increasing rotation until a 'saturation' velocity is achieved, where the chromosphere and coronal loops are fully active. Recent observational results, however, have raised serious questions as to whether this scenario is maintained in low-mass, late-type M dwarfs (Hawley, Reid & Gizis 1999).

The standard rotation/activity hypothesis rests on an extension of the observed behaviour of G and K dwarfs, where there is a clear activity–rotation correlation. Both parameters are believed to be age-dependent, with the star spinning down as it loses angular momentum due to coupling of the star's magnetic field with the local medium (Skumanich 1972). Since activity in these stars is powered by a shell dynamo (Parker 1955), located at the boundary between the radiative core and the outer convective layers, the activity–rotation correlation is expected. This mechanism, however, cannot be present in fully convective low-mass

stars. Indeed, early studies predicted a break in the level of activity at a mass of $\sim 0.3\,M_{\odot}$, where the radiative core disappears. The continued presence of high levels of activity in these stars is probably due to the presence of a turbulent (shear) dynamo mechanism (Durney, De Young & Roxburgh 1993). In that case, there is no expectation of a direct correlation with rotational velocity.

Investigating this question requires a reliable measurement of the level of activity in stars with temperatures between 4000 and 2400 K. The equivalent width of the Hα emission line is frequently used for this purpose. This parameter, however, provides a misleading measure of activity, since the equivalent width produced by a given line flux depends on the level of the underlying continuum. This is a particularly important consideration for M dwarfs, since the R_C-band flux decreases rapidly with decreasing temperature from spectral type M0 ($\sim$4000 K) through M5 ($\sim$2800 K) to M9 ($\sim$2100 K). This complication can be avoided by calculating the parameter $L_{\alpha}/L_{\rm bol}$, the fraction of the total luminosity emitted in Hα. This provides a measure of stellar activity *independent* of both temperature and luminosity.

We have computed bolometric magnitudes for the stars in our sample using the $(V-I)$ colours and the relation

$$BC_I = 0.02 + 0.575(V-I) - 0.155(V-I)^2$$

derived from Leggett et al.'s (1996) data for field M dwarfs. Table 7 lists those magnitudes, together with data for Hyades stars from Stauffer et al. (1997), Jones et al. (1996) and Terndrup et al.

Table 7. Rotation and activity in low-mass Hyades stars.

Name	$v\sin(I)$	$M_{\rm bol}$	$\log(L_{\alpha}/L_{\rm bol})$	Name	$v\sin(i)$	$M_{\rm bol}$	$\log(L_{\alpha}/L_{\rm bol})$
RHy 9	3.5	10.55	−3.88	RHy 23	4	10.08	−3.86
42	3.5	10.19	−3.99	46	5	10.28	−3.89
49	22	9.81	−3.80	60	19	9.66	−3.95
64	19	10.68	−4.01	83	8	11.29	−3.98
98	23	10.68	−3.87	101	16	10.89	−4.14
115	7	10.05	−3.87	119	7.5	10.73	−3.98
126	21	10.36	−3.82	129	3.5	9.94	−3.85
143	4	10.15	−3.85	158	11	10.14	−3.92
162	35	10.59	−3.77	163	19	9.83	−3.94
165	17	11.67	−3.99	182	<3	9.80	−3.87
199	16	10.46	−3.99	200	7.5	10.06	−3.84
202	2.5	10.53	−4.04	219	7	10.55	−3.76
221	2.5	10.50	−3.98	230	16	11.47	−3.91
231	6.5	9.69	−3.73	240A	14.5	11.68	−3.90
240B	14.5	11.72	−4.09	242	6	10.01	−3.93
244	2.5	9.46	−3.76	260	>2.5	10.77	−3.90
281	9.5	11.32	−3.66	297	13	10.52	−3.80
298	6	10.10	−3.86	301	12	10.57	−3.72
331	6.5	10.66	−3.94	346	3.5	10.44	−3.98
367	3	10.11	−3.82	369		10.05	−3.99
371	14	9.23	−3.90	376	4	10.00	−3.83
377	9	9.79	−3.90	386	9	12.00	−3.95
390	18	11.25	−3.77	391	24	9.94	−3.85
399	<2.5	9.64	−3.89	402	11.5	10.94	−3.75
403	5.5	11.10	−3.82				
Jones et al.							
Br 262	37	11.40	−4.08	Br 804	31	11.81	−3.86
Stauffer et al.							
RHy 26	<6	8.96	−3.76	RHy 28	11.5	9.45	−3.87
62	<6	8.28	−4.03	99	<6	9.03	−3.89
100	<6	8.93	−4.35	123	<6	8.69	−5.09
142	11.5	8.42	−3.83	161	<6	9.35	−3.88
189	<6	9.38	−4.66	203	<6	9.09	−5.05
211	6	8.62	−4.39	269	26	8.79	−3.75
283	<6	8.53	−3.93	289	6	9.07	−4.71
294	11	8.79	−3.83	296	<6	9.33	−3.87
322	<6	9.52	−3.35	349	<6	9.11	−3.83
350	<6	10.16	−3.40	384	25	8.52	−3.70
GH 7-33	12.5	8.48	−3.74	Lei 44	18	8.61	−3.63
Lei 73	<6	8.72	−4.86	LP 357-160	<6	8.73	−4.67
LP 358-716	<6	8.93	−4.05	LP 359-2423	9.5	8.79	−3.76
LP 359-262	<6	8.84	−4.55	LP 413-93	<6	9.13	−4.14
LP 535-101	<6	9.09	−4.10	vA 54	<6	8.94	−3.94
vA 106	10	9.16	−3.82				
Terndrup et al.							
RHy 128	19	10.88	−3.86	RHy 138	22	11.66	−3.96
206	24	10.47	−3.93	LP 416-573	6	10.18	−4.01
LP 358-735	25.5	10.16	−3.82	LP 476-648	6	10.18	−3.94
LP 358-717	18	10.64	−3.86				

(2000). Deriving L_α for these stars requires an estimate of the continuum flux at 6563 Å, F_C. Reid, Hawley & Mateo (1995b) demonstrated that F_C can be derived from the R_C-band flux, F_R, from the relation

$$F_C = 1.45F_R.$$

All of the stars in Table 1 have *R*-band photometry (Reid 1993, and references therein). For stars with multiple observations, the Hα fluxes are derived using the average equivalent width (with the exception of the MJD 794.46 observation of RHy 281, discussed further below). Variability, as noted above, leads to typical uncertainties of ± 15 per cent.

The top panel in Fig. 8 shows the [$M_{\rm bol}$, $\log(L_\alpha/L_{\rm bol}$] distribution for Hyades M dwarfs. Contrary to the suggestion by Terndrup et al. (2000), there is no evidence for a decline in activity with decreasing luminosity. Known binaries and single stars are distinguished using different symbols in the diagram, but there is no evidence that the former are more (or less) active than the latter. These data confirm results derived previously by Reid et al. (1995b), a paper which unaccountably seems to have escaped Terndrup et al.'s attention.

Fig. 8(b) plots the [$v\sin(i)$, $M_{\rm bol}$] distribution for the Hyades stars, illustrating the well-known tendency towards higher rotation with decreasing mass. However, Fig. 8(c) shows that there is no correlation between the level of chromospheric activity and rotation: a Hyades M dwarf with $L_\alpha/L_{\rm bol} \sim 1.5 \times 10^{-4}$ can have a measured rotational velocity anywhere between <2 and 40 km s^{-1}, the full range measured for cluster stars.

This result is in good agreement with data for late-type field M dwarfs (Hawley et al. 1999), but directly contradicts Terndrup et al.'s analysis of a subset of the present sample. The origin of the discrepancy rests with Terndrup et al.'s use of equivalent width as an estimator of stellar activity. As noted above (and, indeed, by Terndrup et al.), the equivalent width of an emission line depends on both the total line flux and the level of the local continuum. Thus, early-type Hyades M dwarfs have weaker emission than late-type dwarfs, even though the chromosphere is at the same *proportional* level of activity. Further, Fig. 8(b) shows that late-type dwarfs (with higher Hα EW) tend to have more rapid rotation. Thus the correlation between 'activity' and rotation claimed by Terndrup et al. is actually the [mass/$M_{\rm bol}$, $v\sin(i)$] correlation illustrated in Fig. 8(b).

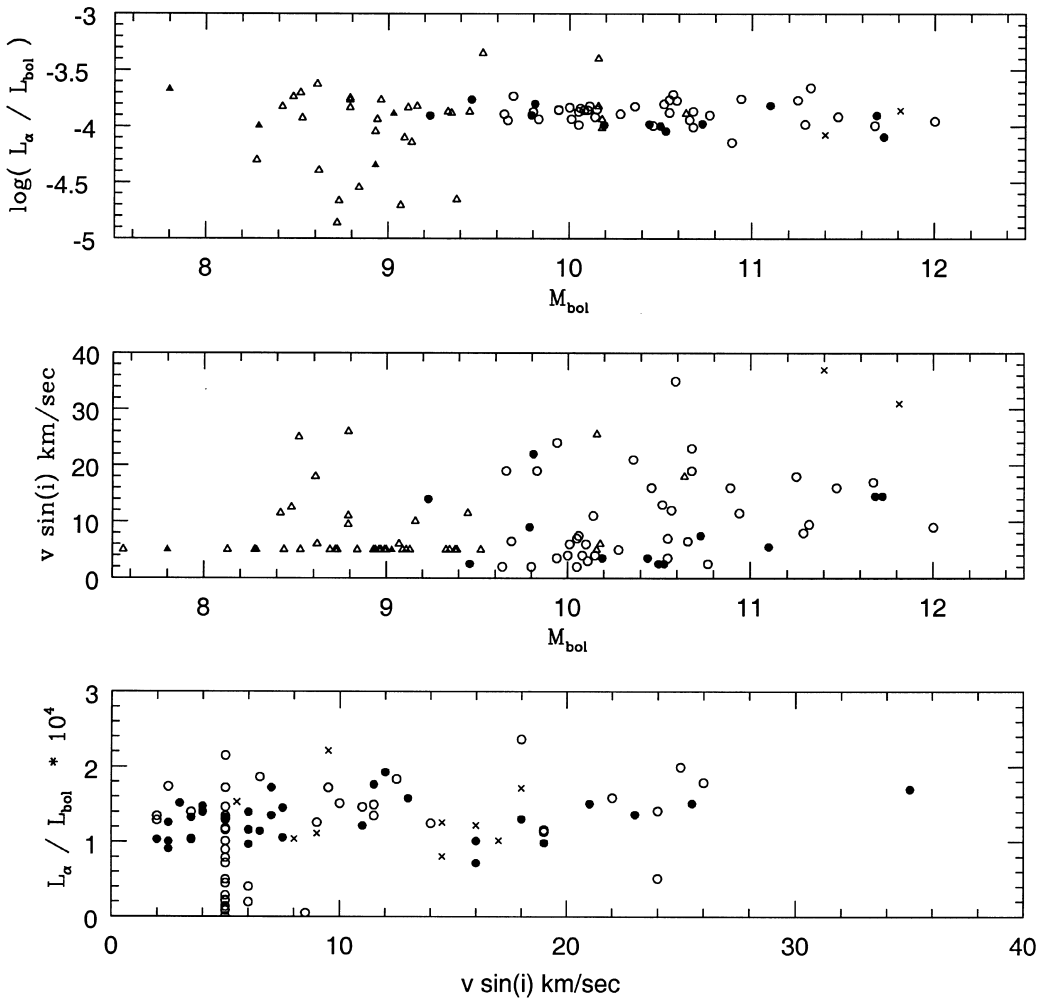

Figure 8. Chromospheric activity and rotation in Hyades dwarfs. The top panel (a) plots activity, $\log L_\alpha/L_{\rm bol}$, for M dwarfs from this paper (circles), and from previous studies (Stauffer et al. 1997; Jones et al. 1996; Terndrup et al. 2000 – all triangles). Solid points mark known binaries. The middle planel (b) plots the [$M_{\rm bol}$, $v\sin(i)$] relation for the same stars, using the same symbols. The bottom panel (c) plots rotation against activity, where all of the Hyades observations are divided into three subsets based on $M_{\rm bol}$. Solid points mark stars with $M_{\rm bol} < 10$; open circles have $10 < M_{\rm bol} < 11$; the faintest stars are marked as crosses.

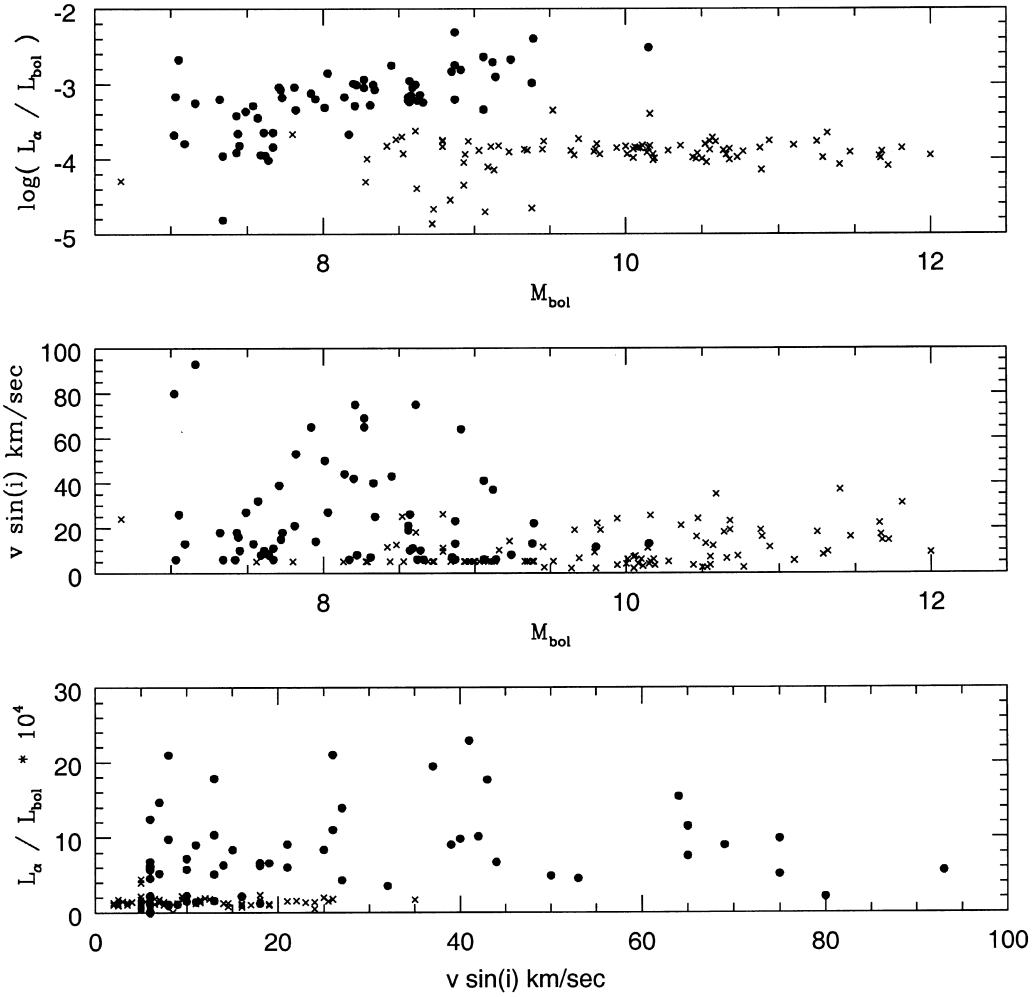

Figure 9. Hα emission and typical cross-correlation results for activity/rotation correlations for Pleiades stars. The data are taken from Basri & Marcy (1995), Jones et al. (1996) and Terndrup et al. (2000) Pleiades stars are plotted as solid points; all Hyades stars from Fig. 8 are plotted as crosses for comparison.

Terndrup et al. also present rotation and activity measurements for low-mass Pleiades stars. Fig. 9 plots their data, together with observations from Basri & Marcy (1995) and Jones et al. (1996), using $L_\alpha/L_{\rm bol}$ rather than Hα EWs.[2] With an age of $\sim$120 Myr, the Pleiades stars are more luminous (and hotter) at a given mass, and significantly more active. Thus the mass range is $\sim 0.1 < M/{\rm M}_\odot < 0.6$, similar to the Hyades stars. While the measured rotational velocities approach 100 km s^{-1}, there is no evidence for any correlation between rotation and the level of chromospheric activity.

These results are consistent with Hawley et al.'s (1999) proposal that the mechanism driving chromospheric activity changes as one moves from early-type M dwarfs to mid- and late-type dwarfs. As convection becomes increasingly important and the radiative core shrinks, the shell dynamo weakens. In contrast, the turbulent dynamo increases in strength, supplanting the shell dynamo entirely in fully convective stars. As a result, rotation is irrelevant to the level of activity present in dwarfs of spectral type M3 and later.

6.2 The flare on RHy 281

One observation in Table 5 stands out: on 1997 December 12, the measured equivalent width of Hα emission in RHy 281 is $\sim$23 Å. As Fig. 10 shows, we happened to catch the star during a flare outburst. In addition to Hα emission, He I 6678 Å is present with an equivalent width of 1.15 Å, core emission is detectable in the K I 7665/7699 doublet, and we measure equivalent widths of 0.85 and 0.35 Å for the 8500 and 8663 Å components of the Ca II near-infrared triplet.

Since our observations concentrated almost exclusively on stars within a narrow range of absolute magnitude, $11.5 < M_V < 16$, we can derive an approximate estimate of the frequency of flare outbursts in these stars. In total, we expended $\sim$67 000 s integrating on M dwarfs in the course of this project; the RHy 281 flare was detected in an 1800 second exposure, and we assume that the flare persisted at a detectable level for the duration of the exposure. Given that assumption, we deduce that low-mass Hyades dwarfs are in outburst for $\sim$2.5 per cent of the time. This compares with an upper limit of $<$7 per cent for the duty cycle estimated for the M9 field dwarf, BRI 0021 (Reid et al. 1999).

7 SUMMARY AND CONCLUSIONS

We have obtained high-resolution spectroscopy of 51 low-mass dwarfs in the Hyades cluster. At least three are confirmed as

[2] Note that using $(V-I)$ instead of $M_{\rm bol}$ in these diagram does not change the overall morphology.

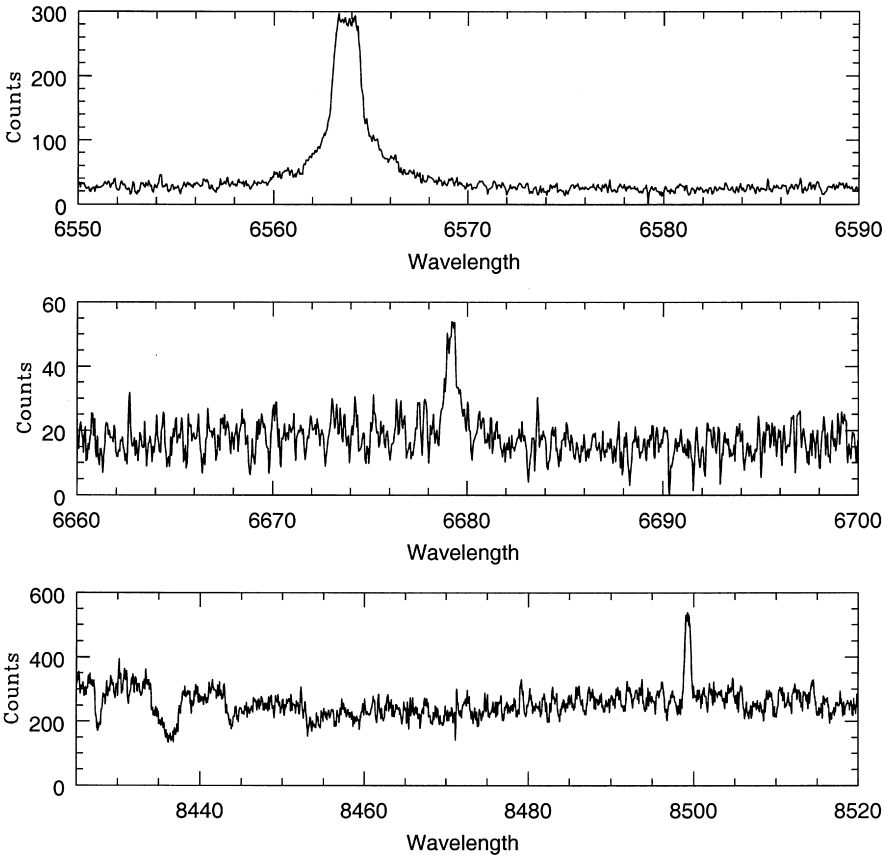

Figure 10. Hα, He I 6678-Å and Ca II 8500-Å emission during the flare outburst of RHy 281.

spectroscopic binaries: two double-lined systems, RHy 42 and 244, the latter previously identified as a binary in *HST* imaging; and RHy 403, a short-period single-lined system with an extremely low-mass secondary. Based on the mass function for the last star and the absence of any detection of the secondary at 8000 Å, we infer mass limits of $0.07 \leq M/\mathrm{M}_{\odot} \leq 0.095$, making this unseen companion a strong brown dwarf candidate.

Four other stars are possible binaries: RHy 158 shows strong indications of velocity variability; RHy 281 lies $\sim 6\,\mathrm{km\,s^{-1}}$ from the expected velocity of Hyades members; RHy 221 and 377 are also offset in velocity, although to a smaller extent. Three further stars have unusual cross-correlation functions, although it is not clear whether these stem from binarity or rapid rotation. Combining the new discoveries with previous *HST* and ground-based identifications, we derive a binary fraction for Hyades M dwarfs of 23 to 30 per cent, similar to results derived from nearby field M dwarfs.

We have also used our data to determine rotational velocities and explore possible correlations between chromospheric activity and rotation. Combined with literature data, we find that the level of chromospheric activity, as measured by the fractional luminosity emitted in the Hα line, $L_{\alpha}/L_{\mathrm{bol}}$, is nearly constant for M dwarfs with $8 < M_{\mathrm{bol}} < 12$. There is no evidence for a significant correlation between activity and rotation as measured by $v\sin(i)$. We interpret this as confirmation that the rotational dynamo is not present in fully convective mid- and late-type M dwarfs. Activity is probably driven by a shear dynamo mechanism, as proposed by Hawley et al. (1999).

ACKNOWLEDGMENTS

Funding for SM was provided by STScI Grant GO-08146.01-97A. INR would like to thank Wal Sargent for the allocation of Keck time in 1999 December. This analysis is based on observations obtained at the W. M. Keck Observatory, which is operated by the California Association for Research in Astronomy, a partnership of the University of California, the California Institute of Technology and the National Aeronautics and Space Administration. The observatory was made possible by a generous grant from the W. M. Keck Foundation.

REFERENCES

Basri G., Marcy G. W., 1995, AJ, 109, 762
Bryja C., Humphreys R. M., Jones T. J., 1994, AJ, 107, 246
Burrows A., Hubbard W. B., Saumon D., Lunine J. I., 1993, ApJ, 406, 158
Cochran W. D., Hatzes A. P., 1999, Div. Planetary Sci. Meeting Am. Astron. Soc., 31, 0902
Delfosse X., Forveille T., Perrier C., Mayor M., 1998, A&A, 331, 581
Duquennoy A., Mayor M., 1991, A&A, 248, 485
Durney B. R., De Young D. S., Roxburgh I., 1993, Sol. Phys., 145, 207
Fischer D. A., Marcy G. W., 1992, ApJ, 396, 178
Giclas H. L., Burnham R., Thomas N. C., 1972, The Lowell Observatory Proper Motion Survey, Lowell Obs. Bull. 158
Gizis J. E., Reid I. N., 1995, AJ, 110, 1248
Gray D. F., 1982, The Observation and Analysis of Stellar Photospheres. Cambridge Univ. Press, New York
Griffin R. F., Gunn J. E., Zimmerman B. A., Griffin R. E. M., 1988, AJ, 96, 172

Hagen H.-J., Groote D., Engels D., Reimers D., 1995, A&AS, 111, 195
Hanson R. B., 1975, AJ, 80, 379
Hawley S. L., Reid I. N., Gizis J. E., 1999, in Griffiths C., Marley M., eds, ASP Conf. Ser., Workshop on Cool Stars and Giant Planets. Astron. Soc. Pac., San Francisco
Henry T. J., 1990, PhD thesis, Univ. Arizona
Henry T. J., McCarthy D. W., 1993, AJ, 106, 773
Jones B. F., Fischer D. A., Stauffer J. R., 1996, AJ, 112, 1562
Leggett D. K., 1992, ApJS, 82, 351
Leggett S. K., Harris H. C., Dahn C. C., 1994, AJ, 108, 944
Leggett S. K., Allard F., Berriman G., Dahn C. C., Hauschildt P., 1996, ApJS, 104, 117
Marcy G. W., Benitz K. J., 1989, ApJ, 344, 441
Marcy G. W., Butler R. P., 1992, PASP, 104, 270
Parker E. N., 1955, ApJ, 122, 293
Patience J., Ghez A. M., Reid I. N., Weinberger A. J., Matthews K., 1998, AJ, 115, 1972
Perryman M. A. C. et al., 1998, A&A, 331, 81
Reid I. N., 1992, MNRAS, 257, 257
Reid I. N., 1993, MNRAS, 265, 785
Reid I. N., Gizis J. E., 1997a, AJ, 113, 2246
Reid I. N., Gizis J. E., 1997b, AJ, 114
Reid I. N., Hawley S. L., 2000, AJ, 117, 343
Reid I. N., Hawley S. L., Gizis J. E., 1995a, AJ, 110, 1838
Reid I. N., Hawley S. L., Mateo M., 1995b, MNRAS, 272, 828
Reid I. N., Kirkpatrick J. D., Gizis J. E., Liebert J., 1999, ApJ, 527, L105
Sandage A., Kowal C., 1986, AJ, 91, 1140
Skumanich A., 1972, ApJ, 171, 565
Stauffer J. R., Balachandran A. C., Krishnamurthi A., Pinsonneault M., Terndrup D. M., Stern R. A., 1997, ApJ, 475, 604
Stern R. A., Schmitt J. H. M. M., Pye J. P., Hodgkin S. T., Stauffer J. R., Simon T., 1994, ApJ, 427, 808
Terndrup D. M., Stauffer J. R., Pinsonneault M. H., Sills A., Yuan Y., Jones B. F., Fiscer D., Krishnamurthi A., 2000, AJ, 119, 1303
Tonry J., Davis M., 1979, AJ, 84, 1511
Vogt S. S. et al., 1994, S.P.I.E., 2198, 362

This paper has been typeset from a TEX/LATEX file prepared by the author.